Synthesis and thermoelectric properties of Mn-doped $AgSbTe_2$ compounds*

Zhang He(张 贺)[a)b)], Luo Jun(骆 军)[b)†], Zhu Hang-Tian(朱航天)[b)], Liu Quan-Lin(刘泉林)[a)], Liang Jing-Kui(梁敬魁)[b)], Li Jing-Bo(李静波)[b)], and Liu Guang-Yao(刘广耀)[b)]

[a)] *State Key Laboratory for Advanced Metals and Materials, School of Materials Science and Engineering, University of Science and Technology Beijing, Beijing* 100083, *China*

[b)] *Beijing National Laboratory for Condensed Matter Physics, Institute of Physics, Chinese Academy of Sciences, Beijing* 100190, *China*

(Received 5 April 2012; revised manuscript received 19 June 2012)

Polycrystalline p-type $Ag_{0.9}Sb_{1.1-x}Mn_xTe_{2.05}$ (x = 0.05, 0.10, and 0.20) compounds have been prepared by a combined process of melt-quenching and spark plasma sintering. The sample composition of $Ag_{0.9}Sb_{1.1-x}Mn_xTe_{2.05}$ has been specially designed in order to achieve the doping effect by replacing part of Sb with Mn and to present the uniformly dispersed Ag_2Te phase in the matrix by adding insufficient Te, which is beneficial for optimizing the electrical transport properties and enhancing the phonon scattering effect. All the samples have the NaCl-type structure according to our X-ray powder diffraction analysis. After the treatment of spark plasma sintering, only the sample with $x = 0.20$ has a small amount of $MnTe_2$ impurities. The thermal analysis indicates that a tiny amount of Ag_2Te phase exists in all these samples. The presence of the $MnTe_2$ impurity with high resistance and high thermal conductivity leads to the deteriorative thermoelectric performance of the sample with $x = 0.20$ due to the decreased electrical transport properties and the increased thermal conductivity. In contrast, the sample with $x = 0.10$ exhibits enhanced thermoeletric properties due to the Mn-doping effect. A dimensionless thermoelectric figure of merit of 1.2 is attained for the sample with $x = 0.10$ at 573 K, showing promising thermoelectric properties in the medium temperature range.

Keywords: $AgSbTe_2$, phase stability, crystal structure, thermoelectric properties

PACS: 61.05.cp, 64.60.My, 73.50.Lw **DOI:** 10.1088/1674-1056/21/10/106101

1. Introduction

Thermoelectric (TE) materials have attracted much attention due to their ability to directly/reversibly convert heat energy into electrical power, which may play a key role in power generation and solid-state cooling.[1−11] TE devices using electrons/holes as the working fluid are environmentally friendly with the advantages of long life, reliability, silent operation, etc.[7,8] The performance of TE materials is measured by a dimensionless TE figure of merit, $ZT = S^2\sigma T/k$, where S, σ, k, and T are the Seebeck coefficient (or thermopower), the electrical conductivity, the thermal conductivity, and the absolute temperature, respectively.[5] Based on the above equation, high-performance TE materials should have high electrical conductivity, large Seebeck coefficient, and low thermal conductivity.

As a p-type compound, $AgSbTe_2$ has been intensively investigated over the temperature range from 300 K to 700 K[12−14] due to its relatively low thermal conductivity (0.6 $W\cdot m^{-1}\cdot K^{-1}$–0.7 $W\cdot m^{-1}\cdot K^{-1}$) and large Seebeck coefficient ($\sim$ 200 $\mu V\cdot K^{-1}$).[12,15] $AgSbTe_2$ has an NaCl-type crystal structure with the space group $Fm\bar{3}m$, in which Te occupies the crystal site of Cl while Ag and Sb distribute randomly on the Na site.[16] According to the previous report,[17] the disordered distribution of Ag and Sb leads to a dramatically reduced lattice thermal conductivity of $AgSbTe_2$ through umklapp and intrinsic phonon–phonon scattering processes without any reduction in the electrical conductivity. Recently, the $AgSbTe_2$ compound has also been used as an important component to construct the so-called bulk nanostructured TE materials with excellent TE properties, such as $(PbTe)_m(AgSbTe_2)$ (denoted as LAST-m) and $(GeTe)_x(AgTeSb_2)_{100-x}$ (named as TAGS-x). The ZT value of LAST-m reaches 2.2 at 800 K when m is 18.[4] The TAGS-x has a ZT value over 1.5 at 800 K when x is 80 or 85.[18]

*Project supported by the National Natural Science Foundation of China (Grant Nos. 11144002 and 51172276).

†Corresponding author. E-mail: jluo@aphy.iphy.ac.cn

© 2012 Chinese Physical Society and IOP Publishing Ltd

According to the pseudo-binary phase diagram of the $y$$Ag_2Te$-(1-$y$)$Sb_2Te_3$ system,[19,20] the stoichiometric $AgSbTe_2$ compound (δ phase with the NaCl-type structure) with $y = 0.5$ does not exist.[21,22] Instead, a single-phase δ region can appear at high temperature with $y = 0.37$–0.47, which decomposes into Sb_2Te_3 and Ag_2Te below 633 K.[15,20,23] In this work, our sample composition has been specially designed to achieve the promising TE performance in the medium temperature range. Firstly, the Ag–Sb–Te alloy with y= 0.45, corresponding to $Ag_{0.9}Sb_{1.1}Te_{2.1}$, has been selected as the ideal composition to obtain the δ phase. Secondly, insufficient Te has been added in order to form a small amount of uniformly dispersed Ag_2Te phase in the matrix, which is effective in reducing the lattice thermal conductivity.[24] Thirdly, Sb is partly replaced by Mn in order to lower the lattice thermal conductivity by the alloying effect and to increase the carrier concentration by the doping effect. Finally, the $Ag_{0.9}Sb_{1.1-x}Mn_xTe_{2.05}$ samples with $x = 0.05$, 0.10, and 0.20 are synthesized by the combined quenching and annealing approach. In this paper, we show that the $Ag_{0.9}Sb_{1.1-x}Mn_xTe_{2.05}$ sample has the promising TE performance and is quite stable below 540 K, which may find applications in the medium temperature range.

2. Experimental details

The elements Ag (99.99%), Sb (99.999%), Te (99.999%), and Mn (99.5%) were used as the starting materials. Materials were weighed and mixed as the nominal composition of $Ag_{0.9}Sb_{1.1-x}Mn_xTe_{2.05}$ ($x = 0.05$, 0.10, and 0.20), then sealed in an evacuated quartz tube ($\sim 10^{-3}$ Pa). The quartz tube was placed vertically in a well-type muffle furnace and held at 1023 K for 12 h, which was then quenched by immersion in water. The quenched sample was annealed at 773 K for a week. The sample for TE property measurement was obtained by spark plasma sintering (SPS) at 623 K for 5 min with a heating rate of 50 K/min under an axial pressure of 50 MPa. Relative densities of all samples were about 97%.

Phase identification and structural analysis were carried out by X-ray powder diffraction (XRD) using a PANalytical X′Pert PRO diffractometer with the Cu $K_{\alpha 1}$ radiation. The Seebeck coefficient and the electrical conductivity were measured by using the four-point probe method using a TE measurement system (ZEM-2, ULVAC). The thermal analysis by differential scanning calorimetry (DSC) was performed on a TA-Q200 analyzer with a heating rate of 10 K/min. The specific heat C_P was obtained by the modulated DSC (MDSC, TA-Q200) with a heating rate of 3 K/min. The thermal diffusivity was measured by the flash diffusivity method (LFA 427, Netzsch). Thermal conductivity κ was calculated using the equation $\kappa = \lambda C_P \rho$, where λ, C_P, and ρ were the thermal diffusivity, the specific heat, and the density, respectively.

3. Results and discussion

3.1. Phase stability and crystal structure

Figure 1(a) shows XRD patterns of the quench-annealed $Ag_{0.9}Sb_{1.1-x}Mn_xTe_{2.05}$ samples, which are consistent with the $AgSbTe_2$ standard card (JCPDS No. 15-0540) without any noticeable secondary phase. As shown in the inset of Fig. 1(a), the diffraction peak shifts to higher 2θ angles with increasing x, indicating that the lattice parameter decreases with the increasing Mn content. According to our Rietveld refinement, the lattice parameters are 6.0797(2) Å (1 Å=0.1 nm), 6.0719(4) Å, and 6.0611(5) Å for $x = 0.05$, 0.10, and 0.20, respectively. This nearly linear decrease of the

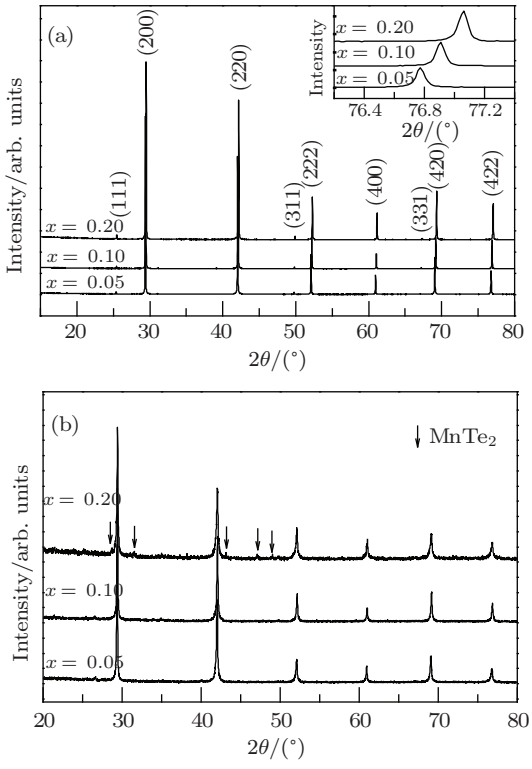


Fig. 1. XRD patterns of (a) quench-annealed and (b) SPS treated $Ag_{0.9}Sb_{1.1-x}Mn_xTe_{2.05}$ samples. The inset shows that the diffraction peak shifts to higher 2θ angles with increasing x.

lattice parameter with the increasing Mn content is expected, since the radius of Mn^{3+} (0.66 Å) is smaller than that of Sb^{3+} (0.76 Å), which implies that Mn^{3+} indeed replaces Sb^{3+} in the crystal lattice.

In order to measure the TE properties, the quenched-annealed samples have been treated by the SPS. Figure 1(b) shows the XRD patterns of the SPS treated samples. For the samples with $x = 0.05$ and 0.10, the diffraction peaks are in accordance with that of the $AgSbTe_2$ compound (JCPDS No. 15-0540) with the NaCl-type structure, and no impurities are observed. However, as the content of Mn increases to $x = 0.20$, a small amount of cubic $MnTe_2$ (JCPDS-18-0813) coexists with the main phase. According to our thermal analysis shown below, the appearence of $MnTe_2$ is attributed to the SPS treatment at 623 K.

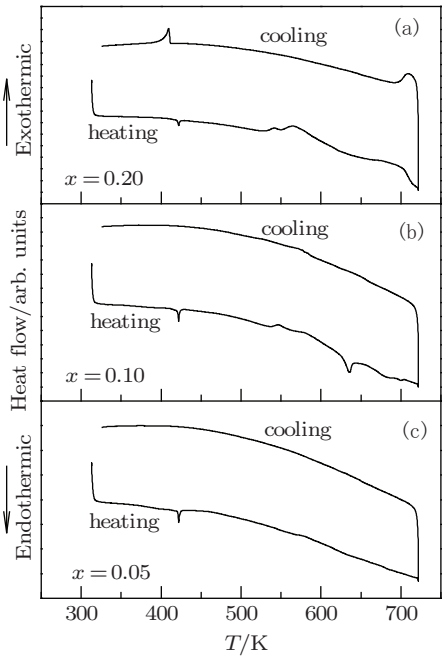


Fig. 2. DSC curves of $Ag_{0.9}Sb_{1.1-x}Mn_xTe_{2.05}$ ((a) $x = 0.20$, (b) $x = 0.10$, (c) $x = 0.05$) samples.

The phase stability of the quench-annealed sample has been analysized by a combined DSC and XRD study. The experimental process is as follows. The DSC measurement is performed on a heating mode; When the appointed temperature (573 K, 648 K, and 723 K) is reached, the sample heating is stopped immediately; After the sample is cooled to room temperature, the sample is collected to carry out the phase identification by using the XRD technique. Figure 2 shows the full-cycle DSC curves of the samples. An endothermic peak at 422 K, corresponding to the phase transition from monoclinic α-Ag_2Te to cubic β-Ag_2Te,[25,26] is observed on the heating DSC curves for all these samples, indicating that our composition design and sample preparation are effective in producing minor Ag_2Te phase in the matrix. However, no diffraction peaks of Ag_2Te are observed on the XRD patterns, because the XRD technique may not be sensitive enough to detect this very small amount of Ag_2Te phase. For the sample with $x = 0.05$, no other phase transition is detected in our meaured temperature range, which is also confirmed by the XRD analysis shown in Fig. 3.

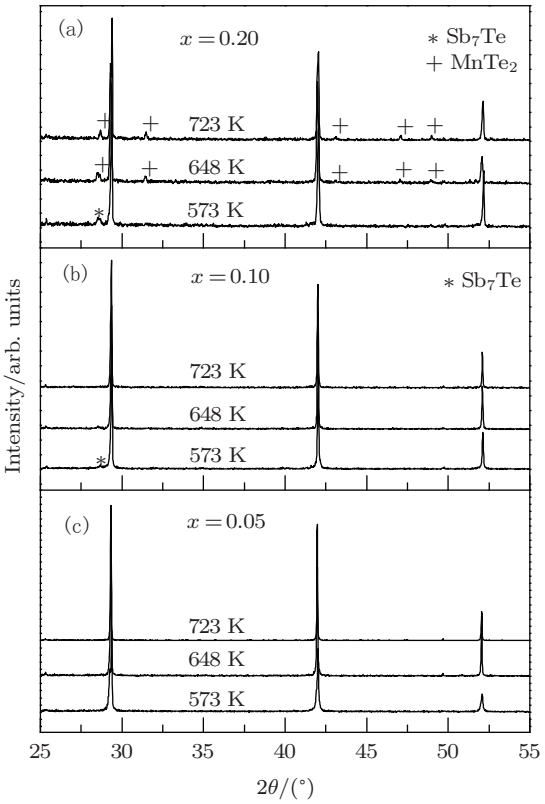


Fig. 3. XRD paptterns of $Ag_{0.9}Sb_{1.1-x}Mn_xTe_{2.05}$ ((a) $x = 0.20$, (b) $x = 0.10$, (c) $x = 0.05$) samples after the DSC measurements to different temperatures.

Based on the combined analysis of the DSC curves (Fig. 2) and the corresponding XRD patterns at the different temperatures (Fig. 3), the other peaks on the DSC curves of the samples with $x = 0.10$ and 0.20 can also be clearly assigned to specific phase transitions. The exothermic peak around 545 K on the heating DSC curves is responsible for the appearance of the unstable phase Sb_7Te, which is the same to the Cu-doped $AgSbTe_2$.[27] The exothermic peak at 566 K is related to the precipitation of $MnTe_2$ in the sample with $x = 0.20$, but this peak is absent in the sample with $x = 0.10$, since this sample has no precipitated $MnTe_2$. The endothermic peak at 635 K for the sample with $x = 0.10$ is corresponding to the disappear-

ance of the unstable phase Sb_7Te, but this peak becomes indistinct and broad (between 615 K and 675 K) for the sample with $x = 0.20$.

3.2. Electrical transport properties

Figure 4 shows the temperature dependences of the electrical transport properties of $Ag_{0.9}Sb_{1.1-x}Mn_xTe_{2.05}$ samples. As expected, the sample with higer electrical conductivity has a lower Seebeck coefficient, and the trend of the S versus T curve is basically consistent with that of the σ versus T curve (see Figs. 4(a) and 4(b)). The positive Seebeck coefficients of all specimens indicate their p-type transport behaviors. The temperature dependences of the electrical conducitivity and the Seebeck coefficient of the sample with $x = 0.05$ are almost the same to that of the non-doped $AgSbTe_2$ sample, in which the electrical transport properties are considered to be influenced by the Ag_2Te impurity.[17] The increased electrical conducitivity and the decreased Seebeck coefficient of the sample with $x = 0.10$ can be ascribed to the increased carrier concentration due to the Mn-doping effect, which is similar to that in the

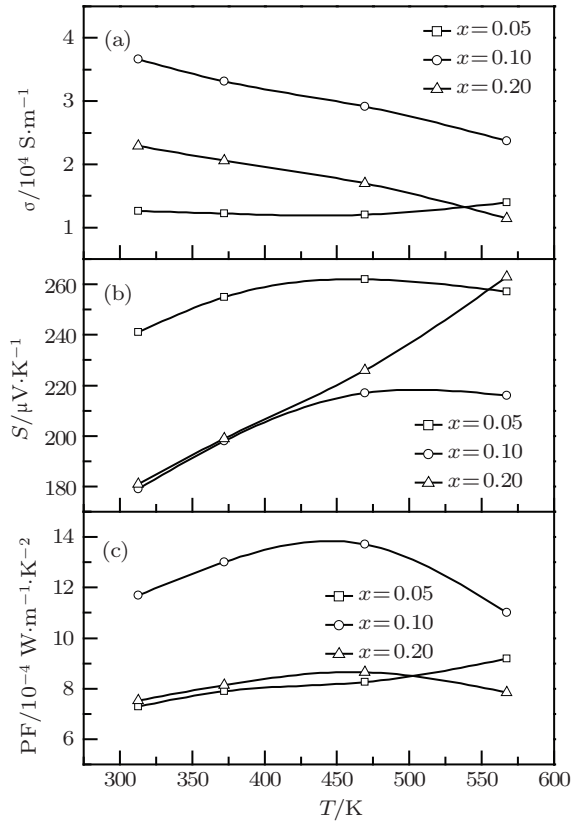


Fig. 4. Temperature dependences of (a) electrical conductivity, (b) Seebeck coefficient, and (c) power factor of $Ag_{0.9}Sb_{1.1-x}Mn_xTe_{2.05}$.

Se-doped $AgSbTe_2$ sample.[17] For the sample with $x = 0.20$, the presence of the $MnTe_2$ second phase with very poor electrical conductivity ($\sim 2.6\times10^2$ S·m^{-1} at 473 K)[28] leads to deteriorative electrical transport properties. Therefore, as shown in Fig. 4(c), the sample with $x = 0.10$ has the highest power factor (PF) $S^2\sigma$ among the three samples. A maximum PF value about 1.37×10^{-3} W·m^{-1}·K^{-2} is attained in the sample with $x = 0.10$ at 473 K.

3.3. Thermal transport properties

Figure 5(a) shows the temperature dependence of the thermal conductivity of the $Ag_{0.9}Sb_{1.1-x}Mn_xTe_{2.05}$ samples. For all specimens, the thermal conductivity first increases, reaches a maximum, and then decreases rapidly with the increasing temperature. The thermal conductivity of the sample with $x = 0.10$ is lower than that of the samples with $x = 0.05$ and $x = 0.20$. Using the Wiedmann–Franz law, $\kappa_e = \sigma LT$, the lattice thermal conductivity κ_l can be estimated by subtracting the electronic thermal conductivity κ_e from the total thermal conductivity κ, $\kappa_l = \kappa - \kappa_e$, where $L = 0.7L_0$ and $L_0 = \pi^2/3(\kappa_B/e)^2 = 2.45 \times 10^{-8}$ V^2·K^{-2} (κ_B is the Boltzmann's constant).[5] As shown in Fig. 5(b), the electronic thermal conductivities of these samples are consistent with their electrical conductivities, i.e., the sample with a higher electrical conductivity also has a higher electronic thermal conductivity. The electronic thermal conductivity of the sample with $x = 0.10$ is larger than that of the sample with $x = 0.05$ due to the higher carrier cenctration of the sample with $x = 0.10$ from the Mn-doping effect. For the sample with $x = 0.20$, the effective carrier concentration is decreased due to the formation of the $MnTe_2$ impurity, thus the electronic thermal conductivity κ_e is also lower than that of the sample with $x = 0.10$.

Figure 5(c) shows the temperature dependence of the lattice thermal conductivity of the $Ag_{0.9}Sb_{1.1-x}Mn_xTe_{2.05}$ sample. Due to the alloy effect, the sample with $x = 0.10$ has a lattice thermal conducitivity lower than that of the sample with $x = 0.05$. A minimum value of 0.3 W·m^{-1}·K^{-1}, approaching the theoretical minimum thermal conductivity,[29] is achieved at 573 K for the sample with $x = 0.10$ due to the alloy effect and the presence of the Ag_2Te impurity. According to the previous report,[24] the Ag_2Te phase dispersed in the matrix is effective on en-

hancing the phonon scattering. From Figs. 5(b) and 5(c), it is obviously that the total thermal conductivity of this system is dominated by the lattice thermal conductivity. Therefore, the sample with $x = 0.10$ shows a total thermal conductivity lower than that of the sample with $x = 0.05$ despite that its electronic thermal conductivity is over twice of that of the sample with $x = 0.05$. The sample with $x = 0.20$ has the largest thermal conductivity, which could be ascribed to the presence of the $MnTe_2$ pricipiatation with higher thermal conducitivity (1.6 $W{\cdot}m^{-1}{\cdot}K^{-1}$ at room temperature).[30]

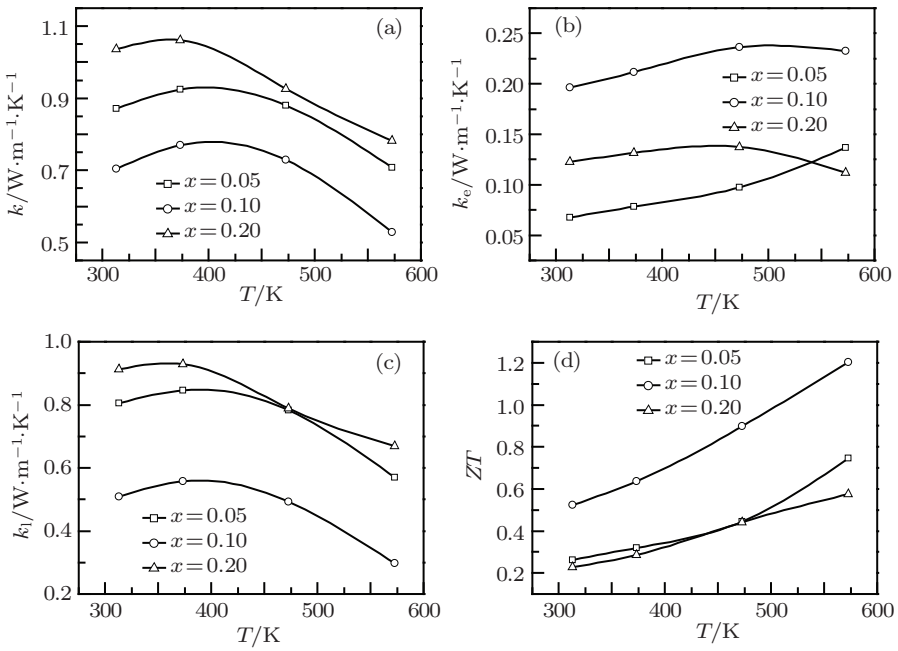


Fig. 5. (a) Total, (b) electronic, and (c) lattice thermal conducitivities and (d) ZT values of $Ag_{0.9}Sb_{1.1-x}Mn_xTe_{2.05}$.

Figure 5(d) shows the temperature dependence of ZT of $Ag_{0.9}Sb_{1.1-x}Mn_xTe_{2.05}$. The ZT values of all samples increase with the increasing temperature. The largest ZT value of 1.2 is attained at 573 K for the sample with $x = 0.10$. Comparing with the undoped $AgSbTe_2$, an increase about 10% in the ZT value is obtained for the sample with $x = 0.10$ over the temperature range from 450 K to 573 K,[17] which may find applications in the medium temperature range or be used as the beneficial complement for the commercial Bi_2Te_3 TE materials.[31–35]

4. Conclusion

Crystal structure, phase stability, and TE properties of $Ag_{0.9}Sb_{1.1-x}Mn_xTe_{2.05}$ compounds have been investigated. The XRD analysis indicates that the quench-annealed samples are single phase compounds with the NaCl-type structure. After the SPS treatment, a small amount of $MnTe_2$ is precipitated in the sample with $x = 0.20$. According to our thermal analysis, all the three specimens are quite stable below 540 K, but phase transitions are detected with further increasing temperature. Particularly, the presence of $MnTe_2$ with high resistance and high thermal conductivity results in deteriorative TE properties of the sample with $x = 0.20$. The best TE performance is achieved for the sample with $x = 0.10$, since the substitution of Mn for Sb leads to the increased carrier concentration and the enhanced phonon scattering. A ZT value of 1.2 is obtained at 573 K for the sample with $x = 0.10$, which shows the promising TE performance in the medium temperature range.

Acknowledgment

We thank Prof. Li Jun-Qin (College of Materials Science and Engineering, Shenzhen University, China) for the SPS treatment and electrical transport properties measurement.

References

[1] Wood C 1988 *Rep. Prog. Phys.* **51** 459

[2] Tritt T M 1999 *Science* **283** 804

[3] Venkatasubramanian R, Siivola E, Colpitts T and O'Quinn B 2001 *Nature* **413** 597

[4] Hsu K F, Loo S, Guo F, Chen W, Dyck J S, Uher S, Hogan T, Polychroniadis E K and Kanatzidis M G 2004 *Science* **303** 818

[5] Rowe D M 2006 *Thermoelectrics Handbook: Macro to Nano* (Boca Raton, FL: CRC/Taylor and Francis) p. 1

[6] Poudel B, Hao Q, Ma Y, Lan Y, Minnich A, Yu B, Yan X, Wang D, Muto A, Vashaee D, Chen X Y, Liu J M, Dresselhaus M S, Chen G and Ren Z F 2008 *Science* **320** 634

[7] Heremans J P, Jovovic V, Toberer E S, Saramat A, Kurosaki K, Charoenphakdee A, Yamanaka S and Snyder G J 2008 *Science* **321** 554

[8] Bell L E 2008 *Science* **321** 1457

[9] Biswas K, He J Q, Zhang Q C, Wang G Y, Uher C, Dravid V P and Kanatzidis M G 2011 *Nat. Chem.* **3** 160

[10] Kraemer D, Poudel B, Feng H P, Caylor J C, Yu B, Yan X, Ma Y, Wang X W, Wang D Z, Muto A, McEnaney K, Chiesa M, Ren Z F and Chen G 2011 *Nat. Mater.* **10** 532

[11] Pei Y Z, Shi X Y, LaLonde A, Wang H, Chen L D and Snyder G J 2011 *Nature* **473** 66

[12] Morelli D T, Jovovic V and Heremans J P 2008 *Phys. Rev. Lett.* **101** 035901

[13] Wang H, Li J F, Nan C W, Zhou M, Liu W S, Zhang B P and Kita T 2006 *Appl. Phys. Lett.* **88** 092104

[14] Jovovic V and Heremans J P 2008 *Phys. Rev.* B **77** 245204

[15] Wojciechowski K T and Schmidt M 2009 *Phys. Rev.* B **79** 184202

[16] Ye L H, Hoang K, Freeman A J, Mahanti S D, He J, Tritt T M and Kanatzidis M G 2008 *Phys. Rev.* B **77** 245203

[17] Du B L, Li H, Xu J J, Tang X F and Uher C 2010 *Chem. Mater.* **22** 5521

[18] Yang S H, Zhu T J, Sun T, He J, Zhang S N and Zhao X B 2008 *Nanotechnology* **19** 245707

[19] Marin R M, Brun G and Tedenac J C 1985 *J. Mater. Sci.* **20** 730

[20] Petzow G and Effenberg G 1988 *Ternary Alloys* Vol. 2 (Weinheim: Wiley-VCH Verlag) pp. 552–555

[21] McHugh J P, Tiller W A, Haszko S E and Wernick J H 1962 *J. Appl. Phys.* **32** 1785

[22] Majer R G 1963 *Zeitschrift fur Metallkunde* **54** 311

[23] Ayralmarin R M, Brun G, Maurin M and Tedenac J C 1990 *Eur. J. Solid State Inorg. Chem.* **27** 747

[24] Zhang S N, Zhu T J, Yang S H, Yu C and Zhao X B 2010 *J. Alloys Compd.* **499** 215

[25] Wang H, Li J F, Zou M M and Sui T 2008 *Appl. Phys. Lett.* **93** 202106

[26] Sugar J D and Medlin D L 2009 *J. Alloys Compd.* **478** 75

[27] Zhang H, Luo J, Zhu H T, Liu Q L, Liang J K and Rao G H 2012 *Acta Phys. Sin.* **61** 086101 (in Chinese)

[28] Avdeev B V, Yu P and Krasheninin 1974 *Sov. Phys. Solid State* **15** 2028

[29] Cahill D G, Watson S K and Pohl R O 1962 *Phys. Rev.* B **46** 6131

[30] Johnston W D, Miller R C and Damon G H 1965 *J. Less-Common Met.* **8** 272

[31] Zhao X B, Ji X H, Zhang T H, Zhu T J, Tu J P and Zhang X B 2008 *Appl. Phys. Lett.* **86** 062111

[32] Tang X, Xie W J, Li H, Zhao W Y, Zhang Q J and Niino M 2007 *Appl. Phys. Lett.* **90** 012102

[33] Im J T, Hartwig K T and Sharp J 2004 *Acta Mater.* **52** 49

[34] Jiang J, Chen L D, Bai S Q, Yao Q and Wang Q 2005 *Mater. Sci. Eng.* B **117** 314

[35] Ma Y, Hao Q, Poudel B, Lan Y C, Yu B, Wang D Z, Chen G and Ren Z F 2008 *Nano. Lett.* **8** 2580